CHAPTER 6

TRIBOLOGICAL PERFORMANCE OF NANOCOMPOSITE DLC COATINGS

6.1 INTRODUCTION

The surface condition of a load-bearing component is usually the most important engineering factor. It is almost inevitably the outer surface of a work-piece that is subjected to wear and corrosion while it is in use. Since the time of Leonardo da Vinci (1452-1519) who was arguably the first engineer to study friction and wear in detail, surface and coatings technology have become an important branch of modern surface sciences and engineering. Due to the complexity of wear processes combining individual physical events between sliding surfaces, it is still however a challenge to understand the precise mechanisms of friction and wear on the micrometer scale. Nevertheless, the economic aspects of friction and wear drive an increasing research effort in the development of coatings that might exhibit a combination of very low friction and low wear rates for applications in sliding and rolling contact.

A panoply of testing techniques has been developed to examine the tribological performance of PVD coatings. While the actual applications of DLC coatings in the automotive industry are often under lubricated contacts, tribological tests without lubricants and in ambient air or controlled atmospheres allow the investigation of the physical mechanisms that affect self-lubrication effects. The results of these tests do not always guarantee that a coating will be successful in a particular application, but they assist in determining the mode of wear of different coating materials in the stage of coating design and development. The well defined loading conditions employed in laboratory tests may be different from those of real applications where lubricant and even abrasive particles are often present. Indeed, abrasive wear resistance is of paramount importance in many tribological applications, and so is the interaction of the oil and oil additives with the coating material. Nevertheless, the present study concentrates on pure sliding wear performance. The temperature of the coated components in the contact is also an important factor influencing the tribological behavior of the coatings. For this reason, annealing experiments and high temperature wear tests were performed to investigate modifications of the coating mechanical properties and tribological performance due to temperature, respectively. The thermal stability of the substrate material is also important in this sense in that the substrate needs to maintain its mechanical properties to properly support the coating in the contact. The mechanical properties of the high speed M2 tool steel substrate material used in this thesis are maintained up to temperatures of at least 400 °C, and other substrate materials such as nitrided steels have comparable resistance to temperature since the nitriding treatment is typically carried out at a temperature of 450-550 °C. Other

substrate materials such as bearing steels (e.g. 100Cr6 steel (SAE 52100)) can be heat-treated at temperatures as low as 180 degrees, so that they will be limited in their thermal stability during use.

DLC-based coatings may exhibit low friction, which has been attributed to the possible formation of a transfer layer on the surface of the uncoated counterpart. Recent research has paid some attention to the effects of transfer films on friction behavior, but their importance is still rather overlooked.[1] The friction behavior of hydrogenated and hydrogen-free DLCs differs in the formation mechanism of transfer films within the contact.[2] The former makes the contact between two similar hydrophobic DLC surfaces and in the latter a graphitic layer acts as solid lubricant. The influence of environment on the friction of diamond like carbon based materials is a topic of controversy and remains under continuous debate. Contradictory reports can be found of the effects of adsorbed gases on the friction coefficient. For example, Zaïdi et al. observed that the steady-state coefficient of friction (CoF) of graphite fell as the partial pressure of oxygen gas increased or as the sliding velocity decreased.[3]. In contrast, Heimberg et al. noted that adsorbed gases appeared to increase the CoF of hydrogenated DLC films.[4] Obviously, the surface characteristics of materials play a crucial role in the tribological performance. The influence of the adsorption of N_2 gas by DLC material during dry sliding experiments, causing a variation of friction coefficient with sliding speed and with time, has been explained by some authors through the use of the Elovich equation. The same equation can also describe our experimental results if only the adsorption of water vapor is considered. This will be commented in section 6.5. The friction behavior of TiC/DLC nanocomposite coatings is more complicated compared with pure DLCs. It will be shown that the presence of TiC nanocrystallites influences the formation of transfer layer, and in the case where the DLC matrix cannot efficiently shield TiC particles in the transfer films, as in the case of nanocomposite coatings with a large volumetric fraction of TiC nanocrystallites, TiC nanoparticles may hamper the formation of the transfer layer. In this chapter the formation of the transfer layer and its affecting factors are studied in detail for the hydrogenated TiC/DLC coatings described in chapters 3 and 4.

6.2 SELF-LUBRICATION AND FORMATION OF TRANSFER LAYER

Representative graphs of friction coefficient versus running laps are shown in Fig. 6.1, where three different kinds of friction behavior of the nanocomposite coatings are recognized. Coating 0V110 exhibits a nearly constant coefficient of friction (CoF) and the coating 100V80 shows rather large fluctuations in the friction coefficient curve. The mean CoF of the coatings 0V110 and 100V80 is above 0.2, i.e. much higher than that of the rest four coatings. All four remaining coatings show not only a low steady-state CoF (0.047-0.069), but also a quick drop in the CoF from an initially high value of about 0.2 at the beginning of sliding until the transition point where the steady state is reached. This behavior is attributed to the gradual formation of a transfer film on the counterpart surface during the early stage of a tribo-test, which makes the contact in between two basically similar hydrophobic DLC surfaces that contribute to self-lubrication. Against different counterparts, i.e. sapphire, alumina and bearing steel balls, only slight differences in the friction coefficient are observed on the coatings with self-lubrication (Fig. 6.1b). It may imply that the interfacial sliding actually takes place between the transfer films on the ball

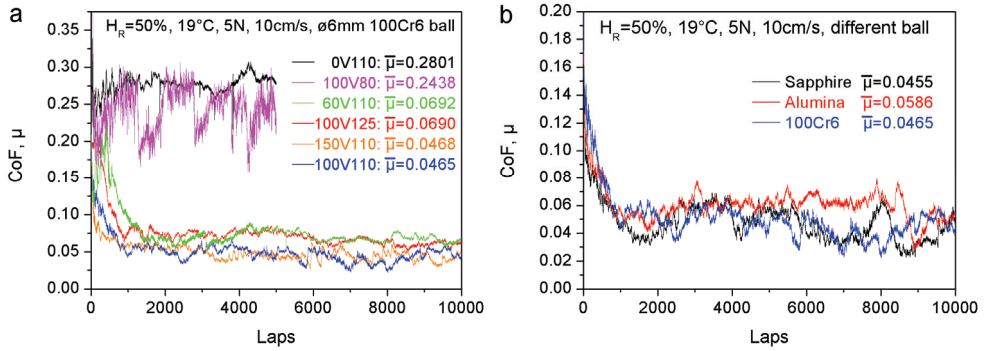

Figure 6.1 *CoF graphs of nc-TiC/DLC nanocomposite coatings: (a) three characteristic friction behaviors recognized on the coating 0V110, 100V80 and the other four coatings; (b) friction graphs of the coating 100V110 sliding against different balls.*

and the surface of the coating, rather than sliding between the surfaces of the counterpart and the coating.

To prove that the self-lubrication is induced by the formation of transfer films, experiments were done in such a way that a fresh surface area of the ball was placed on the same wear track after the stationary state was reached. The friction coefficient immediately jumped up to a value that characterizes the friction between the fresh steel surface and the coating, as seen in Fig. 6.2a. Again, the friction coefficient dropped down quickly as the transfer films were gradually covering the ball surface. Further experiments have been carried out to demonstrate the effect of cleaning the contact area of the ball by rinsing with ethanol and drying with dry N_2. Cleaning resulted in small peaks in the graph of friction coefficient followed by a quick drop in friction again. However, the friction coefficient at the maximum of these peaks is lower than that when a fresh surface of the ball was brought into contact with the wear track, which may be possibly attributed to partially adhered films that could not be cleaned completely. An SEM image of such transfer layer is shown in Fig. 6.2b. The EDX elemental mapping presented in Fig. 6.2c shows that the transfer film contains Ti from the coating; the presence of C was also revealed by EDX analysis.

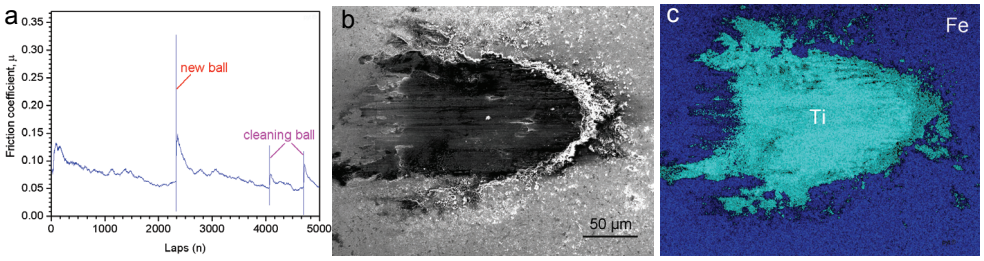

Figure 6.2 *(a) CoF graph of a tribo-test interrupted three times; (b) SEM micrograph of the wear scar of the ball counterpart and (c) Ti and Fe element mapping of the corresponding area.*

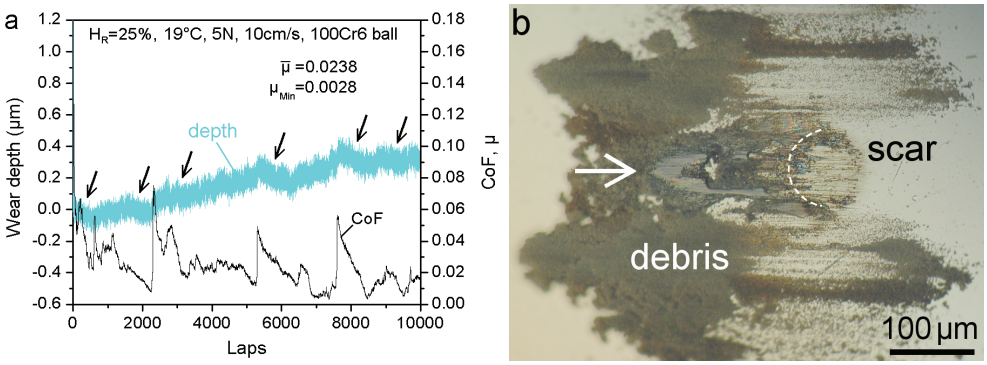

Figure 6.3 *(a) Dynamic frictional behavior of coating 100V110 sliding in air of 25% relative humidity and (b) wear scar of 100Cr6 steel ball with its front border indicated by a dashed line. An arrow indicates the sliding direction of the coating in contact.*

To investigate further the influence of the transfer layer, the wear depth was monitored *in-situ* through an RVDT sensor. Segments with a negative slope were observed in the depth vs. laps graph, as marked by the arrows in Fig. 6.3a. These segments are indicative of the built-up of a transfer layer on the ball surface, rather than a real reduction in the depth of the wear track on the coatings. Correspondingly, substantial drops in the CoF were detected. The maximum growth amplitude in the thickness of the transfer films was measured at about 100 nm and the minimum at the level of 10 nm. Often peaks are observed in the trace. Their presence can be explained as follows: as the transfer film forms on the counterpart, the CoF cannot decrease further and therefore starts to fluctuate. It can be inferred that since the transfer film covers the ball surface in contact, the wear rate of the coating decreases and leads to less wear debris. As a result, the transfer film becomes thinner during sliding until it fully breaks down, leading to a sudden rise of the CoF. Sliding at a higher CoF can generate more debris from the wear track, which in turn can provide the necessary material for the growth of a new transfer film. Thereafter, a new cycle of the dynamic friction process is repeated. Fig. 6.3b shows the wear scar of the 100Cr6 ball covered with a transfer film and also the wear debris collected in front of and beside the wear scar.

6.3 INFLUENCE OF SLIDING VELOCITY

Friction between two surfaces in relative motion is a complex phenomenon that involves phonon dissipation, bond breaking and formation, strain-induced structural transformation and local surface reconstruction, and adhesion. From a physics point of view it is influenced by short- and long-range interactions between the surfaces and it is often accompanied by wear. However, the underpinning mechanism of friction and the up-scaling from atomic phenomena to microscopic effects are still not understood. The two classical friction laws were discovered by da Vinci and Guillaume Amontons, respectively, and were summarized much later by Charles-Augustin Coulomb who also introduced the third friction law. The three laws of friction describe that the friction force in a contact is (i) proportional to the normal force between the surfaces; (ii) independent of the apparent contact area and (iii) independent of the sliding velocity. A remarkable finding of the study

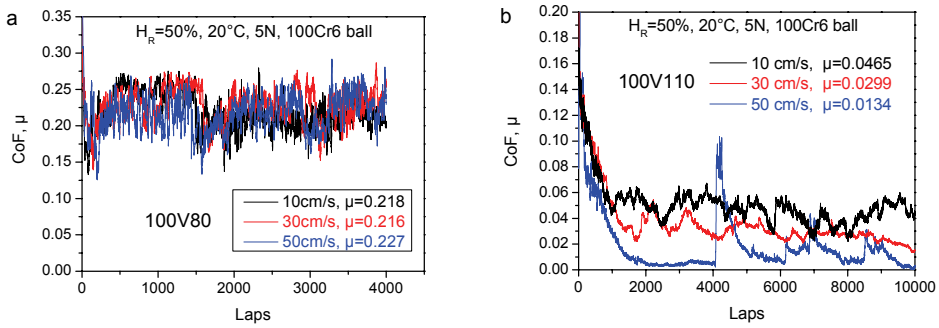

Figure 6.4 *Graph of coefficient of friction versus number of laps of the coatings: (a) 100V80 and (b) 100V110 for dry sliding ball-on-disk experiments against a 100Cr6 steel ball.*

presented here is a breakdown of the Coulomb friction law in the TiC/DLC nanocomposite coatings.

Fig. 6.4 shows graphs of CoF versus the number of laps for coatings 100V80 and 100V110, tested at various sliding velocities. The CoF graphs of coating 100V80 in Fig. 6.4a are nearly horizontal curves with large fluctuations, and the mean values of CoF at different velocities are almost the same, i.e., 0.218, 0.216 and 0.227 at sliding velocities of 10, 30 and 50 cm/s, respectively. Apparently, the coating 100V80 without self-lubricating effect exhibits a CoF that is independent of the sliding velocity. In other words, the Coulomb friction law holds in this case. In contrast, the CoF of coating 100V110 drops quickly from an initial value of about 0.2 at the beginning of sliding to a very low value of CoF (<0.05) at steady state, which is attributed to self-lubricating effects. Especially, a strong dependence of the steady state CoF on the sliding velocity is observed such that the faster the sliding velocity, the smaller the CoF (Fig. 6.4b). The steady state CoF of coating 100V110 at sliding velocities of 10, 30 and 50 cm/s is 0.047, 0.030 and 0.013, respectively. It is clear that the Coulomb friction law is no longer valid when self-lubrication occurs.

The dependence of CoF on the sliding velocity is not affected by the variation of the relative humidity. Two groups of tribotests have been performed on another self-lubricating coating (100V125) at relative humidities of 70% and 50%, respectively, and the results are displayed in Fig. 6.5. A lower CoF is observed at higher sliding velocities, independently of the relative humidity. In addition, sometimes sharp peaks in the friction trace are observed at the highest sliding velocity of 50 cm/s (Figs. 6.4b and 6.5b). The shape of these peaks suggests the sudden removal of the transfer film, followed by a new cycle of transfer film growth that gradually lowers the CoF to the steady state value, as already observed in Fig. 6.2 when the transfer layer was artificially removed from the ball surface. Such a break down of the transfer film at high sliding velocity may lead to a transition from a steady state situation to a metastable sliding condition that results in higher overall CoF and wear rate values. There is therefore a limitation of dry sliding velocity at different levels of humidity, below of which interrupted self-lubrication is retained, such that the CoF is stable and maintains a low value. For instance, the critical velocities of coating 100V110, recorded at 0% and 50% relative humidity, were 10 and 50

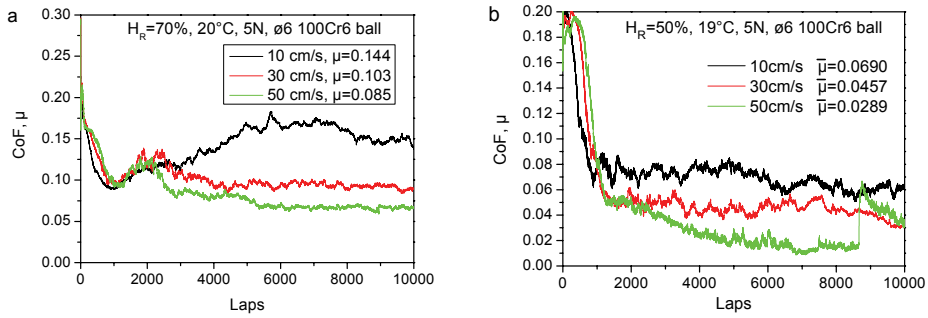

Figure 6.5 *Influence of sliding velocity on the CoF of coating 100V125 tested at different levels of relative humidity (H_R): (a) 70% and (b) 50%.*

cm/s, respectively. In general, sliding is limited to a lower velocity at low humidity, as we will discuss in more detail in the next section.

The different frictional behavior of the nanocomposite coatings is directly reflected in the wear rate of the sliding couples. As shown in Fig. 6.6 b and c, the wear rate and CoF of coatings 100V110 and 100V125 decrease with increasing sliding velocity, while the wear rate of the 100Cr6 ball counterpart stays almost constant. In contrast, coating 100V80 without self-lubricating effects demonstrates little reduction in wear rate, but a significant increase in the wear rate of the 100Cr6 ball counterpart is seen with increasing sliding velocity, despite the fact that the CoF is independent of the sliding velocity.

Since self-lubrication is clearly a consequence of transfer film formation, it is important to examine the morphology of the transfer films formed under the various testing conditions. The CSM tribometer automatically lifts up the loading-arm at the end of a test, before the rotation of the disk sample stops. In order not to disturb the status of the accumulated debris and transfer film on the ball counterpart surface, the counterpart, together with its holder, was carefully removed from the loading-arm and put under an optical microscope for inspection. Typical micrographs of the ball wear scars are shown in Fig. 6.7. A large amount of debris is accumulated in the front and to the sides of the wear scars that are covered with transfer films. The most significant difference among the three tests is the thickness of transfer films and the distribution of the debris around the wear scar. It is clearly revealed using the perspective three-dimensional confocal micrographs in Fig. 6.7 that the transfer films are thinner and looser at higher sliding velocity. In contrast, a thick ridge of transfer film is observed on the middle part of the wear scar in Fig. 6.7a and is spread evenly over the back border of the scar, which may explain the highest CoF measured at the slowest velocity and highest humidity (Fig. 6.5a).

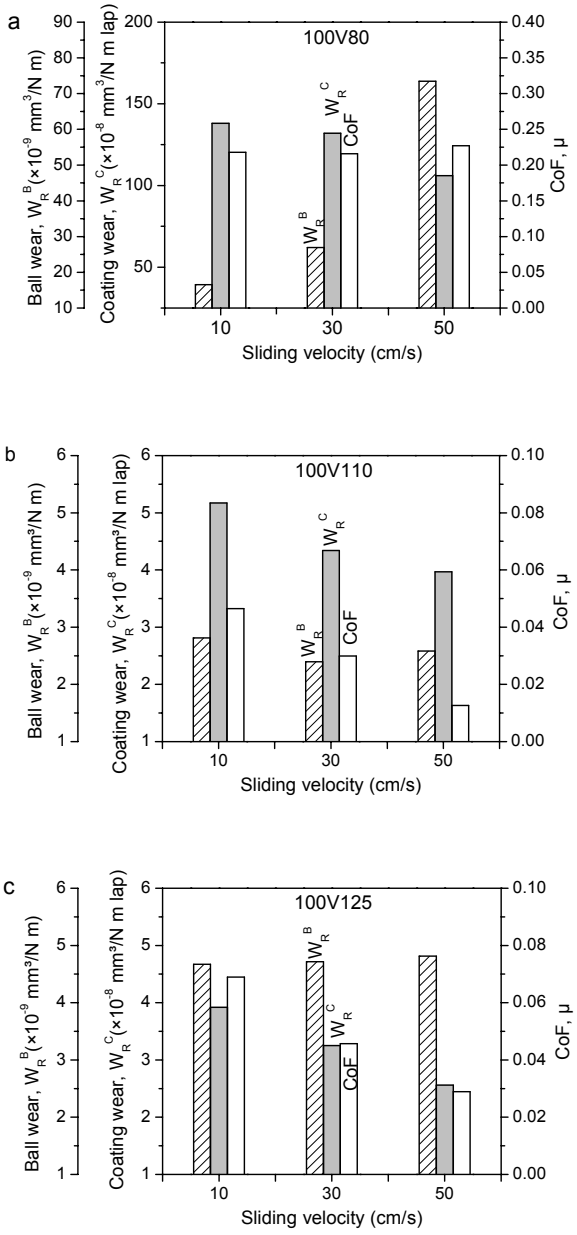

Figure 6.6 *Influence of sliding velocity on the wear rate of 100Cr6 ø6 mm ball counterpart and the nanocomposite coatings: (a) 100V80, (b) 100V110 and (c) 100V125 (5N load, 50% relative humidity and 20°C room temperature). The steady state CoFs are also indicated.*

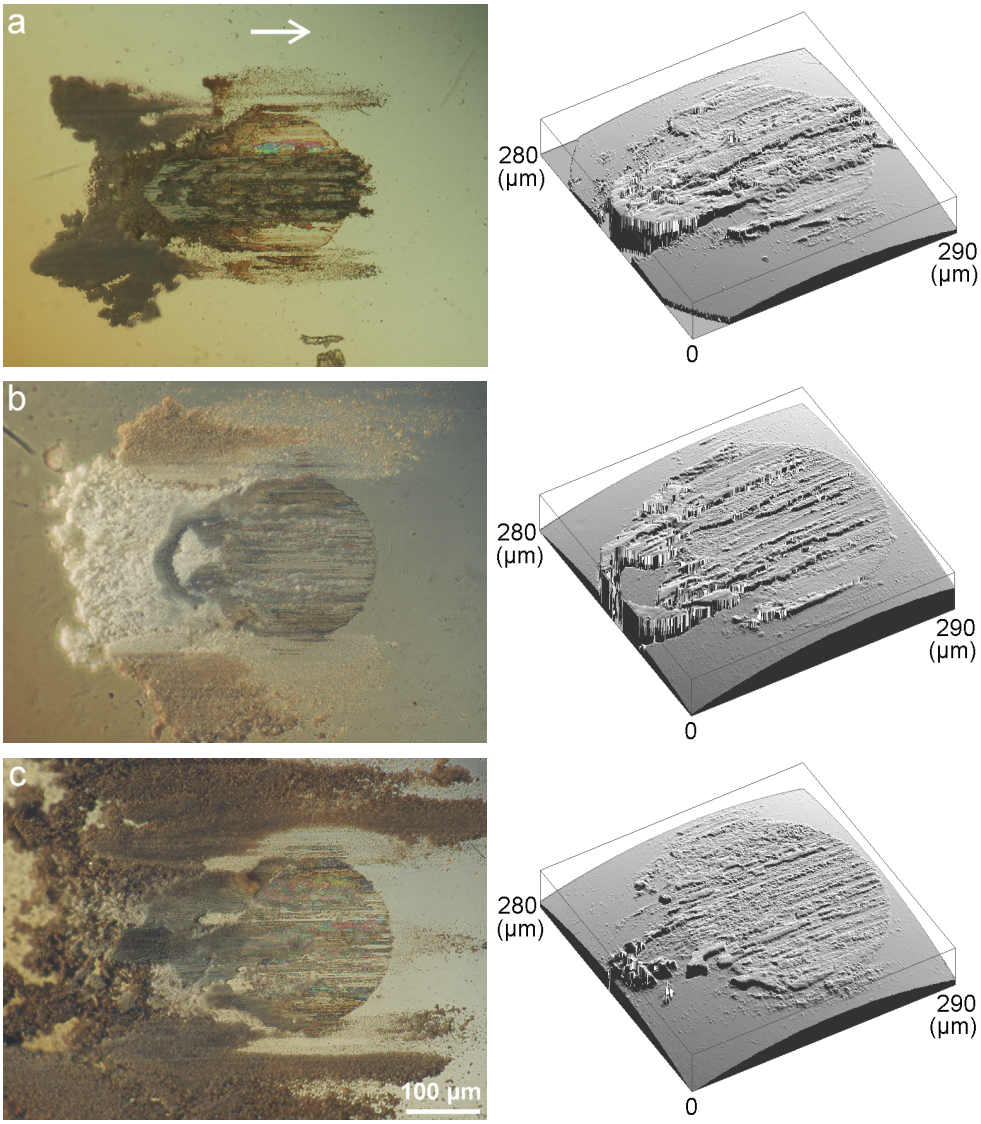

Figure 6.7 *Wear scar of 100Cr6 balls after sliding of 10000 laps against coating 100V125 under 5 N normal load, 70% relative humidity and different sliding velocity: (a) 10 cm/s, (b) 30 cm/s and (c) 50 cm/s. An arrow indicates the sliding direction of the coating in contact. The three dimensional micrographs in the right column are captured with a confocal microscope after cleaning the loose wear debris and correspond to the 2D optical micrographs in the left column.*

Fig. 6.8 shows the wear scar of the 100Cr6 ball counterpart sliding against the coating 100V80. Dense and long scratches parallel to the direction of sliding are distributed over the whole scar. Wear debris from the coating is transferred over the ball surface, but this

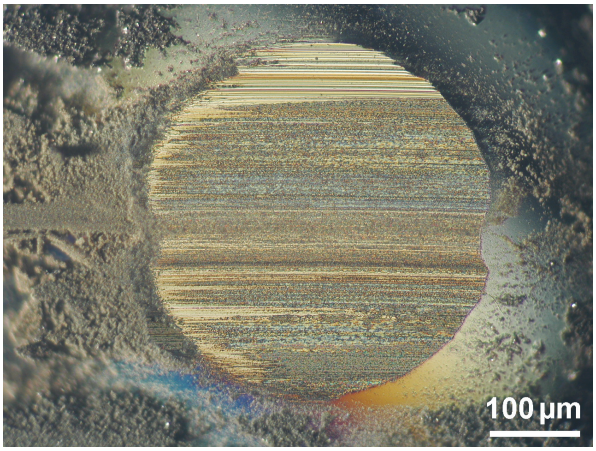

Figure 6.8 *Wear scar of 100Cr6 ball after sliding of 10000 laps against coating 100V80 under the tribo-testing conditions of 5 N normal load, 10 cm/s sliding velocity and 1% relative humidity.*

does not form a transfer layer, therefore self-lubrication is not active. It can be concluded that abrasive wear occurred during the experiment, since the coating is much harder than the ball (20 GPa versus 7.5 GPa) and it is composed of a large volumetric fraction (60 %) of relatively large TiC nano-particles that may act as an abrasive medium.

In the case of non-lubricating coatings such as 100V80 where the Coulomb friction law holds, it was observed that the wear rate of 100Cr6 ball counterparts increases significantly with the sliding velocity, in contrast to the wear rate of the coating itself. To explain this experimental result, the thermal response of the wear couple (100Cr6 bearing steel and the nanocomposite coating) to the flash temperatures in the sliding contact must be considered. Although many models and theoretical considerations on flash temperatures have been proposed during the past decades since Blok's work,[5,6,7] experimental validations of the models are still very difficult. In general, the flash temperature (ΔT) can be estimated using the following expression:[8]

$$\Delta T = \frac{1}{4} \cdot \frac{\mu P v}{(K_1 + K_2) a} \tag{6.1}$$

where μ is the CoF, P the applied normal load, K_1 and K_2 the thermal conductivities of the ball counterpart and the coating, and a is the radius of the real contact area $a = \sqrt{P / \pi H}$, where H is the hardness of the softer material between the coating and the counterpart. The contact temperature is equal to the room temperature (20 °C) plus the flash temperature. The variation of the contact temperature for various values of the friction coefficient, as a function of sliding speed and applied load is shown in Fig. 6.9 *a* and *b*, respectively, assuming a value of 7.5 GPa for the hardness and 17 $Wm^{-1}K^{-1}$ for the thermal conductivity of the 100Cr6 counterpart,[9] and a value of 13.8 $Wm^{-1}K^{-1}$ for the thermal conductivity of the composite coating with a 0.6 V_F of TiC particles.[10,11,12,13]

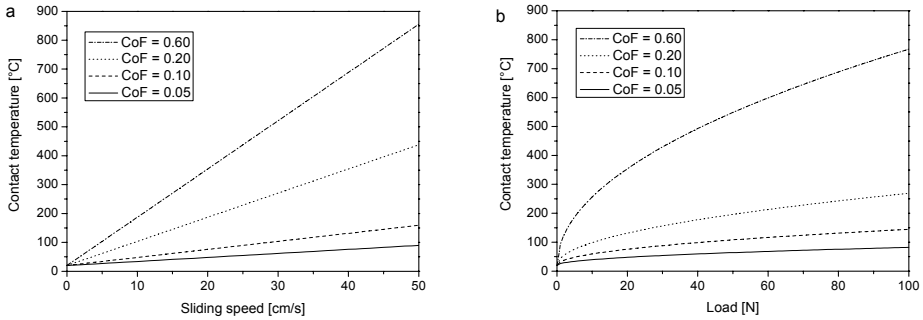

Figure 6.9 *(a) Variation of contact temperature as a function of sliding speed for an applied load of 5 N and different values of friction coefficient (indicated). (b) Variation of contact temperature as a function of the applied load for a sliding speed of 10 cm/s and different values of friction coefficient (indicated).*

It is clear from Fig. 6.9 that both the sliding speed and the applied load have a strong influence on the flash temperatures developing in tribological contacts. Their influence is stronger for high values of friction coefficient, while the application of a self-lubricating DLC coating may decrease the temperature of the counterparts. This effect is so strong that the application of a self-lubricating coating may reduce the extent of degradation of the structural properties of the materials in contact. Also it affects the tribochemical reactions (mainly oxidative) that may increase the wear rate and introduce hard debris in the contact area in the form of metallic oxides. Indeed, in the present case for the non-lubricating coating, such as 100V80, contact temperatures of 82°C, 203°C and 340°C are expected at sliding velocities of 10, 30 and 50 cm/s, respectively. It is known that 100Cr6 bearing steels start to soften at temperatures typically between 180 and 190 °C.[9] Accordingly, the asperities on the wear scar of the 100Cr6 ball are expected to start yielding due to the high temperature at the sliding velocity of 30 cm/s and yield heavily at 50 cm/s. It can be concluded that thermal yielding of the asperities beyond the softening temperature leads to a significant increase in the wear rate of 100Cr6 ball counterpart as the flash temperature becomes higher with increasing sliding velocity. TiC/DLC nanocomposite coatings are thermally stable up to an annealing temperature of 350 °C, with a reduction of less than 10 % in hardness after annealing for one hour at 350 °C in air, as will be shown later. In view of this, a change in the coating wear status due to temperature is not expected in the tests described so far. Furthermore, in tribological tests with a “ball-on-disk“ configuration, the wear scar of the ball is continuously in contact with the coating, whereas the corresponding areas on the coating sample are only periodically in contact, i.e. once for each disk revolution. This implies that the asperities on the wear scar of the ball counterpart undergo continuous thermal loading due to the flash temperature. In contrast, those on the wear track of the coating experience pulsed thermal loading only once per disk revolution from which they can recover in between cycles. Such a dependence of the wear rate of the ball counterpart on the sliding velocity has not been observed for the self-lubricating coatings within the sliding velocity range, because in this case the CoF is nearly 10 times smaller. Much lower flash temperatures are expected in this case, below the softening temperature

of 100Cr6 bearing steel. In addition, the wear scar of the ball is actually covered by the transfer film that acts as a solid lubricant and protects the ball from wear.

6.4 INFLUENCE OF HUMIDITY

The effects of relative humidity on friction are depicted in Fig. 6.10a. In general the CoF of coating 100V110 decreases with decreasing humidity. Moreover, peaks have been recorded in the CoF curves when the relative humidity is equal to 25% or lower and they occur more often in dry air if the sliding velocity stays constant. This implies that the sliding velocity used is close to the limit in dry air and also raises slightly the steady-state CoF . These CoF peaks are attributed to the frequent break down of the transfer film as described in section 6.3. Such a decrease of CoF with humidity has also been observed for coating 100V125, where only a couple of peaks in the CoF curve occurred in dry air so that a monotonic decrease of CoF with decreasing humidity was recorded.[6] By comparing the frequency of the CoF peaks in dry air between the coatings 100V110 and 100V125, it should be pointed out that the critical sliding velocity is also affected by the volumetric fraction of the DLC matrix: the wider the TiC particle separation in the matrix, the higher the critical velocity will be.

The dynamic response of CoF to humidity and the corresponding change in the transfer film thickness are shown in Fig. 6.10. Three levels of relative humidity, i.e. 70%, 30% and 0%, were employed in a single tribotest run, where the transitions from high to low humidity were quickly realized by purging dry air into the testing chamber of the tribometer. During the first part of the tribotest at 70% relative humidity, the frictional behavior of coating 100V125 is just a replica of the results depicted in Fig. 6.5a. It is interesting to note the change of CoF over the humidity transition periods. The CoF drops immediately once the humidity falls. Although the drop of CoF continues after the transition periods, there is a small step in the CoF decay corresponding to the end of the humidity drop as marked by arrows in Fig. 6.10b, after which the slope of the CoF drop is further reduced. This indicates that several different mechanisms are involved in the reduction of the friction. Thickening of the transfer film starts immediately after the humidity drops, and lasts much longer than the transition periods, indicated by the segments of depth curve with a negative slope as shown in Fig. 6.10b. Apparently, this

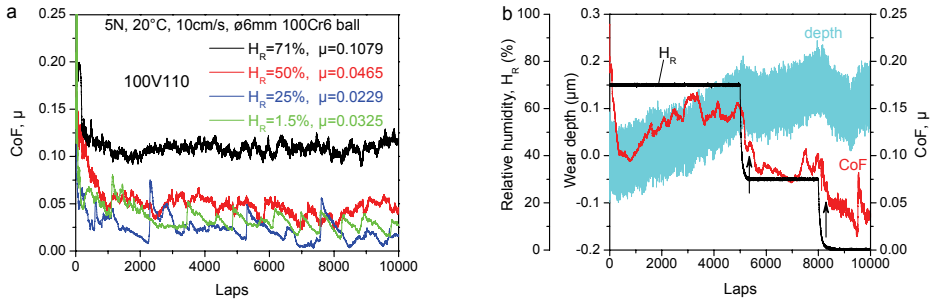

Figure 6.10 (a) *Effects of relative humidity on the CoF of the coating 100V110 and (b)CoF dynamic response to humidity of coating 100V125.*

thickening contributes to the whole course of the CoF drop. On the other hand, the thickness and coverage of the adsorbed water molecular layer on the fresh transfer film and wear track are determined by the relative humidity and decrease as humidity lowers during the transition periods. It is understood that energy dissipation to the water molecular layer will accordingly decrease in the transition periods until a lower level is reached at lower humidity. This transition period is reflected by the first steep decline of CoF before the steps. The two self-lubricating coatings exhibit a rather complicated wear response as a function of the level of humidity, as shown in Fig. 6.11. The wear rates of both the 100V110 coated discs and 100Cr6 ball counterpart decrease with decreasing humidity, with the exception in dry air where the wear rates and CoF increase (Fig. 6.11a).

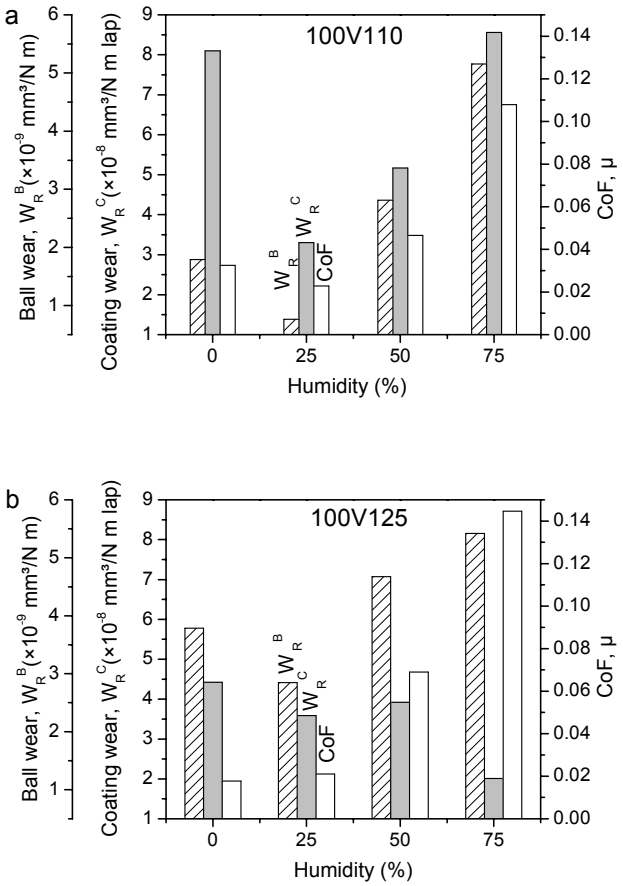

Figure 6.11 *Influence of humidity on the wear rate of 100Cr6 ball counterpart and coatings: (a) 100V110 and (b) 100V125, tested at 5N load, 10cm/s sliding velocity and 20°C.*

This is attributed to the metastable status of wear in dry air as the sliding velocity is beyond the critical velocity, resulting in frequent transfer film breakdown and fluctuations in the degree of self-lubrication, as seen in Figs. 6.10a and 6.4b. The wear rate of coating 100V125 at 75% humidity is obviously lower than that in dry air (Fig. 6.11b) and quite different from the situation of coating 100V110, although the CoF and the wear rate of the ball counterpart exhibit a similar evolution with humidity. It has to be realized that the high volumetric fraction of the DLC matrix in the coating 100V125 enhances the adsorption of water vapor to form quickly an adsorbed molecular layer on the wear track surface after each ball pass. Such a rapidly formed layer of water molecules protects the coating from wear, but at the expense of higher friction. Another effect comes from the extra contribution of the enhanced toughness and high H/E ratio, discussed in section 6.6.

6.5 EFFECTS OF WATER MOLECULAR ADSORPTION ON FRICTION

It was observed in sections 6.3 and 6.4 that a lower humidity and a higher sliding velocity have a similar effect on the frictional behavior of the self-lubricating coatings, i.e. they result in the formation of thinner transfer films that provide a lower friction coefficient. It is expected that both dependencies originate from the same microscopical mechanism, i.e. the influence of the water vapor condensation on the rheology of the transfer layer.

The surface coverage of the adsorbed gas on a solid surface as a function of time (t) can be successfully described empirically using the Elovich equation:[14]

$$\frac{dq}{dt} = Ae^{-\alpha q} \tag{6.2}$$

which can be integrated as:

$$q = \frac{1}{\alpha}\ln(\alpha A) + \frac{1}{\alpha}\ln(t + \frac{\beta}{\alpha A}) \tag{6.3}$$

where α is a constant associated with the number of available adsorption sites over the surface and A is a constant related to the flux of adsorbing gas, which was found to be proportional to its partial pressure in certain cases of non-dissociative adsorption.[15] β is determined by integration of Eq.(6.3) from the initial condition (t_i,q_i) to the situation of (t,q), i.e.:

$$e^{\alpha q_i} - A\alpha t_i = e^{\alpha q} - A\alpha t = \beta \tag{6.4}$$

When at the onset q_i and t_i are taken to be equal to zero, β is equal to unity. In a ball-on-disk tribo-test, each time the ball counterpart passes a point on the circular wear track, it "wipes" a contact area. Thereafter, the contact area is re-exposed to gases in the environment for new adsorption; the exposure time between two successive wipes is inversely proportional to the sliding velocity. Indeed, the time between successive swipes, t, will equal:

$$t = \frac{2\pi \cdot r}{v} \tag{6.5}$$

where r is the radius of the wear track and v is the sliding velocity.

The Elovich equation was employed successfully to interpret the dependency of the friction coefficient of DLC coatings on the exposure time to a dry N_2 atmosphere.[4] In that case the authors employed values of 0.75 for α and values ranging between 0.48 and 3.40 s^{-1} for the constant A, and obtained good fits to their experimental data. In our case it is clear that the parameter governing the frictional behavior of the nanocomposite coatings is the relative humidity, which is directly proportional to the partial pressure of water vapor in the testing atmosphere. The qualitative variation of the fractional coverage of the DLC surface during the ball-on-disk test can be estimated as a function of the relative humidity and the sliding speed, respectively. The variation of fractional coverage as a function of the relative humidity (RH) is shown in Fig. 6.12a for three different sliding speeds. The variation of RH in the interval of 0-100 % was implemented by varying the value of the constant A linearly between 0 and 3.4 s^{-1}. Indeed, other researchers fit their experimental results by varying the value of A between 0.48 and 3.4 s^{-1} according to the partial pressure of N_2 that they employed. Our experimental results indicate that the adsorption of water vapor is responsible for the frictional behavior, and its partial pressure is varied between 0 at RH =0 % and its saturation point at RH=100 % (P_w^*=2332.8 Pa at 20 °C).[16] The variation of the fractional coverage as a function of the sliding speed is shown in Fig. 6.12b and implemented by varying the exposure time t to the atmosphere for different values of relative humidity according to (6.4).

By applying the Elovich equation to our experimental results, it is possible to describe qualitatively the trend of the friction coefficient as a function of relative humidity and sliding speed, as shown in Fig. 6.13 *a* and *b*, respectively. This is an indication that the condensation of water vapor and its influence over the thickness of the transfer films may be responsible for the variation of friction coefficient both as a function of the RH and of the sliding speed.

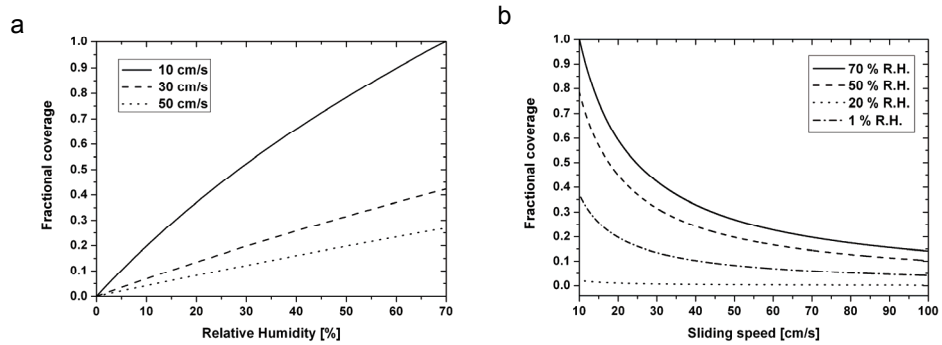

Figure 6.12 *(a) Water vapor fractional coverage of DLC surface as a function of relative humidity, for different sliding speeds (indicated). (b) Water vapor fractional coverage of DLC surface as a function of sliding speed, for different humidity levels (indicated).*

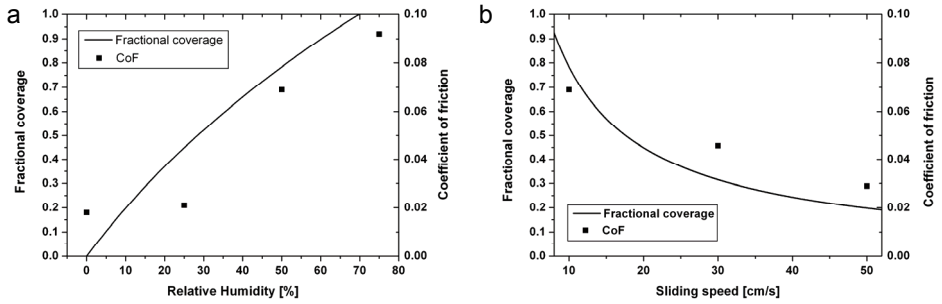

Figure 6.13 *Comparison of the variation of CoF and fractional coverage with (a) the relative humidity and (b) sliding speed.*

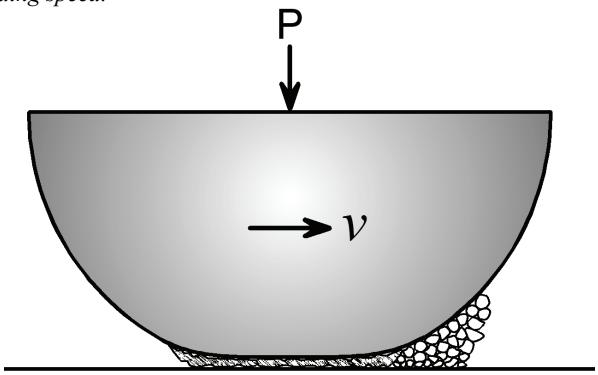

Figure 6.14 *Sketch of accumulated debris and transfer film on the wear scar of ball counterpart. The accumulated debris may collapse in low humidity or dry air beyond the critical sliding velocities, due to less densification at absence of water molecules adsorbed.*

While it was not possible to gather sufficient experimental evidence yet, the following mechanism may be proposed to explain the frictional behavior of the nanocomposite TiC/DLC coatings. The transfer film and the wear debris accumulated at the front of the wear scar of the ball counterpart actually carry the contact load, as sketched in Fig. 6.14; their rheology is of prime importance in lowering the friction. When this nano-sized debris is (in dry air) not covered by water molecules, they may be brought into (and easily sheared at) the sliding interfaces with a very weak interaction between both themselves and the surface of the wear track. However, at high sliding velocity the flow of debris into the sliding contacts may be interrupted due to the collapse of accumulated debris in front of the wear scar. Such collapses lead to the frequent breakdown of transfer films and correspondingly to the peaks of CoF beyond the critical sliding velocity, see Fig. 6.10a. At faster sliding velocity and/or lower level of humidity the films become thinner and looser and therefore they easily break. Collapses of the accumulated debris are expected to be more damaging to the thinner transfer films seen at higher sliding velocities. Condensation of water molecules collected from the surface of the wear track may change the nature of transfer films in humid air. It is well known that adsorbed gases, especially water vapor,

increase the rate of densification of particulate materials, for instance wear debris accumulated here. As seen in Fig. 6.7a, denser and thicker transfer films have been formed at higher humidity and at lower velocity. One can conclude that it requires more energy expenditure (as friction) to slide and smear such a film than a loose and easy to shear one between the sliding surfaces.

6.6 WEAR BEHAVIOR

6.6.1 HYDROGENATED DLC COATINGS

The wear properties of TiC/DLC nanocomposite coatings versus deposition parameters are summarized in Fig. 6.15. Concerning the mechanical properties (Table 6.1), it is clear that the wear rate (W_R) of the nanocomposite coatings decreases significantly with increasing H/E ratio, but not with hardness. A high wear rate is always accompanied by a high coefficient of friction. The coefficient of friction decreases with increasing C content to a minimum value of 0.046 at 110 sccm flow rate of acetylene, but increases again with further increase in C content (flow rate of acetylene). It is understood that the nanocrystalline TiC (*nc*-TiC) particles may serve as a promoter for surface graphitization of the DLC matrix that leads to ultra-low friction. Surface graphitization of the DLC matrix is boosted due to the high localized shear stresses applied by the exposed *nc*-TiC in the transfer films (nano-scaled asperities). On the other hand these TiC nano-crystallites also scratch the coating surface and facilitate wear. There is a trade-off between CoF and wear rate towards the low volume fraction of *nc*-TiC. It is thus understandable that the nanocomposite coatings exhibit even smaller CoFs, than those of pure DLC coatings (typically 0.1~0.15 under comparable conditions of loading and counterpart), where such hard and sharp nano-scaled TiC asperities (promoters) are missing. The importance of such a trade off is that the coatings possessing various combinations of CoF and W_R can be selected for different applications according to whether high wear resistance or low friction is the major concern.

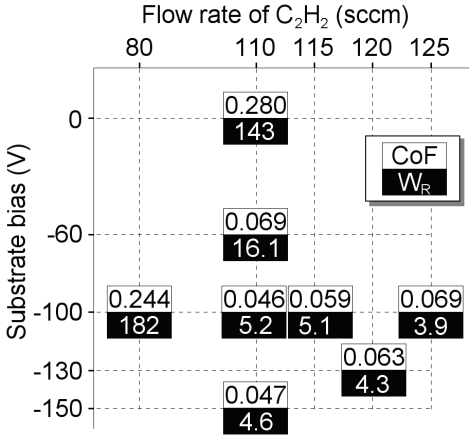

Figure 6.15 *Map of steady-state CoF and wear rate (W_R) in dimension of $\times 10^{-8}$ mm³/N m (per lap) versus the deposition parameters of TiC/DLC nanocomposite coatings under the same tribo-testing conditions: H_R=50 %, 20 °C, 5 N, 10 cm/s, sliding against ø6 mm 100Cr6 ball.*

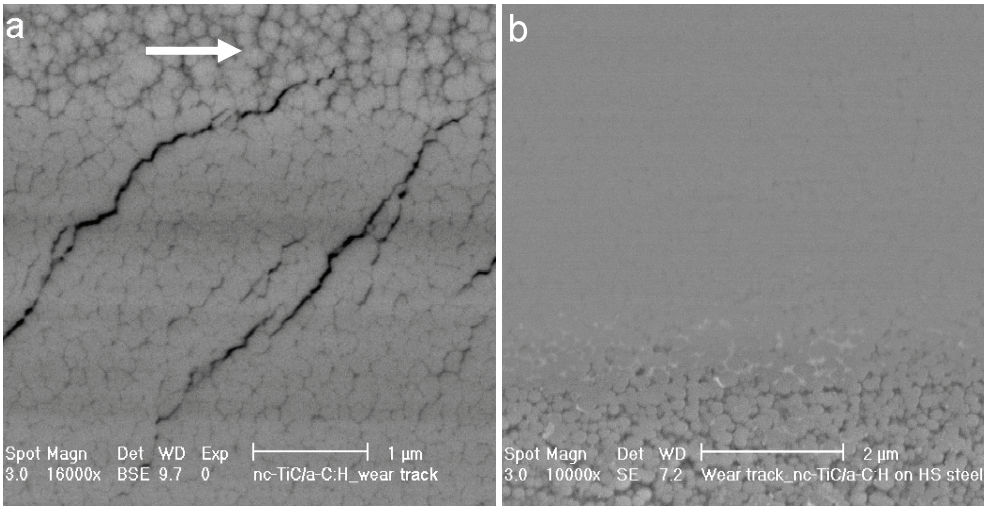

Figure 6.16 *SEM micrographs of the wear tracks: (a) micro-cracks initiate and readily propagate through the columnar boundaries in the coating 100V80 and (b) smooth and featureless wear track formed on the coating 100V125 under the same wear conditions (5N load, 10cm/s sliding speed, T=20°C 50% humidity and against ø6mm 100Cr6 ball). An arrow indicates the movement direction of the counterparts.*

Table 6.1 *Deposition parameter, hardness, H/E* and values of wear rate and friction coefficient for tribotests performed under the same conditions: H_R=50 %, 20 °C, 5 N, 10 cm/s, sliding against ø6mm 100Cr6 ball.*

Coating	Bias [V]	C_2H_2 flow [sccm]	*H* [GPa]	H/E*	W [mm³ / N m lap]	CoF
0V110	0	110	5.5	0.09	140×10^{-8}	0.29
60V110	60	110	11.8	0.11	16×10^{-8}	0.07
100V110	100	110	15.6	0.11	9×10^{-8}	0.05
150V110	150	110	19.8	0.11	5×10^{-8}	0.09
100V80	100	80	20.0	0.08	180×10^{-8}	0.24
100V115	100	115	14.8	0.12	5×10^{-8}	0.06
130V115	130	115	17.4	0.12	6×10^{-8}	0.07
130V120	130	120	17.4	0.12	4×10^{-8}	0.06
100V125	100	125	15.8	0.12	3×10^{-8}	0.07

An important factor that affects the coating wear resistance is the presence of columnar boundaries within the coatings. It is shown in Fig. 6.16a that a coating with thick columnar boundaries such as 100V80 undergoes brittle failure during the tribological test, with numerous cracks propagating along its columnar boundaries. On the other hand, the surface of the wear track of coating 100V125 appears very smooth due to the lack of columnar boundaries and inherently higher toughness.

It was already discussed in chapter 2 that the wear resistance of hard coatings is expected to depend on the H/E parameter, the "elasticity index", rather than on the

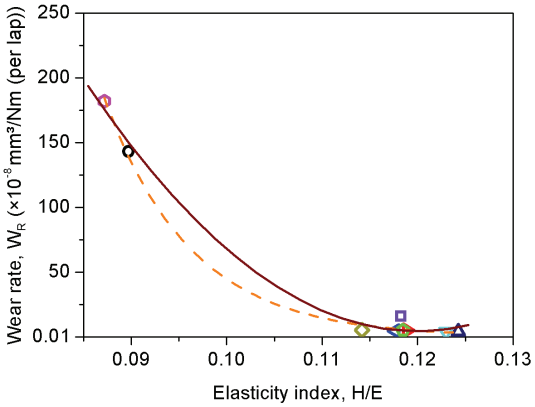

Figure 6.17 *Wear rate versus H/E ratio defined as the elasticity index of TiC/DLC nanocomposite coatings. The solid line represents a fit to a power law H/E dependence up to the second order and the dashed line is the fit to an exponentially decaying function in H/E. Each coating is represented by a different symbol: 0V110 circle, 60V110 square, 100V110 diamond, 150V110 left triangle, 100V80 hexagon, 100V115 right triangle, 100V125 down triangle, 130V115 pentagon and 130V120 up triangle.*

hardness. The variation of wear resistance of the layers as a function of the H/E parameter is plotted in Fig. 6.17 and fitted with a power law or an exponential function, respectively. Both functionalities are able to fit the experimental data, confirming the importance of the H/E parameter in determining the wear resistance of tribological coatings.

INFLUENCE OF ANNEALING ON THE TRIBOLOGICAL PERFORMANCE

In order to reveal the thermal resistance of the coatings, the variation of their hardness and elastic modulus was monitored by nanoindentations experiments after annealing them for one hour at various temperatures in air. Table 6.2 lists the mechanical properties of the annealed coatings.

Table 6.2 *Mechanical properties of nc-TiC/DLC nanocomposite coatings after annealing in air for 1 hour.*

Coating code	Properties	Annealing temperature (°C)						
		20 *	130	200	250	300	350	400
100V115	H (GPa)	14.9				13.2	11.6	6.6
	E (GPa)	124.5				119.4	109.8	102.2
	H/E ratio	0.119				0.111	0.106	0.064
130V115	H (GPa)	17.4	17.3	17.2	17.2	16.7	16.1	
	E (GPa)	146.9	152.1	155.8	147.8	144.3	143.3	
	H/E ratio	0.118	0.114	0.111	0.116	0.116	0.112	
130V120	H (GPa)	17.4				16.3	15.6	
	E (GPa)	140.1				139.2	136.6	
	H/E ratio	0.124				0.117	0.114	
HS steel substrate	HV (GPa)	8.16	8.00	8.06	8.04	8.10	7.90	

* as deposited

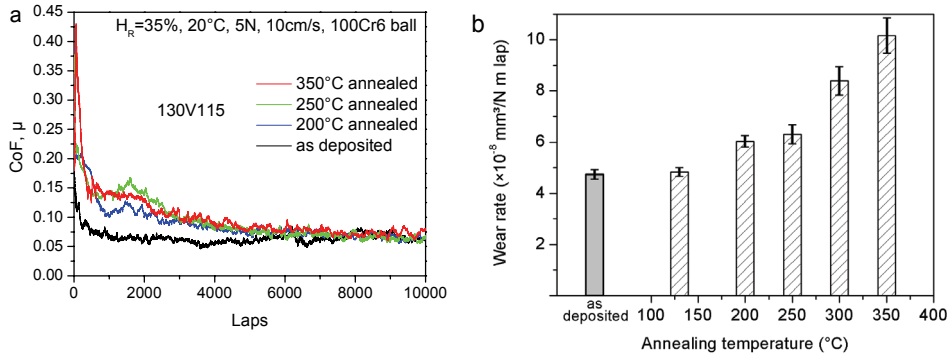

Figure 6.18 *Influence of annealing temperature on the tribological properties of coating 130V115: (a) coefficient of friction (CoF) and (b) wear rate, tested at room temperature and 35% relative humidity, 5 N normal load and 10 cm/s sliding velocity against 100Cr6 ball.*

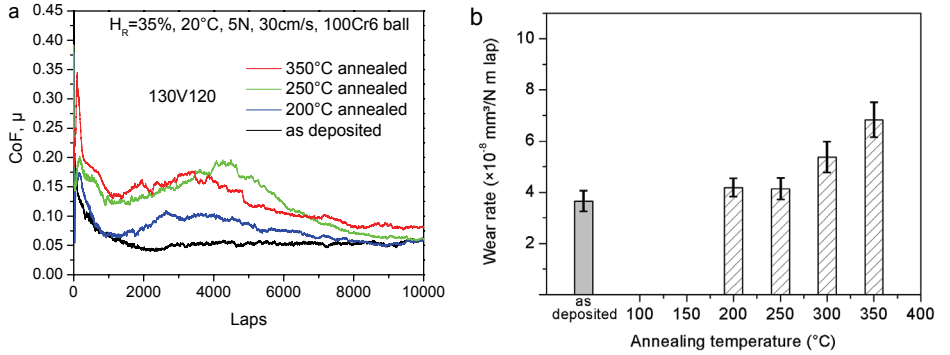

Figure 6.19 *Influence of annealing temperature on the tribological properties of coating 130V120: (a) coefficient of friction (CoF) and (b) wear rate, tested at room temperature and 35% relative humidity, 5 N normal load and 30 cm/s sliding velocity against 100Cr6 ball.*

It is clear that the coatings are thermally stable up to 250°C but start to soften at 300°C. The softening of annealed coatings becomes pronounced above 350°C. In contrast, it is known that the mechanical properties of bearing steels (e.g. 100Cr6) degrade at a temperature of about 190°C. Figures 6.18 and 6.19 demonstrate the tribological performances of the as-deposited and annealed coatings 130V115 and 130V120, respectively, as tested with ball-on-disk dry sliding against ø6 mm 100Cr6 balls under 5 N normal load and 10 cm/s sliding speed.

The as-deposited coatings show the typical self-lubricating behavior observed for the previous coatings. That is to say, the coefficient of friction (CoF) drops from an initially high value of about 0.2 at the beginning of sliding to a low steady-state CoF of about 0.06-0.08, after a transition period during which transfer films gradually form over the surface of the ball counterpart. The wear rate of the annealed coatings remains quite stable up to the annealing temperature of 250°C and increases significantly when annealed at temperatures

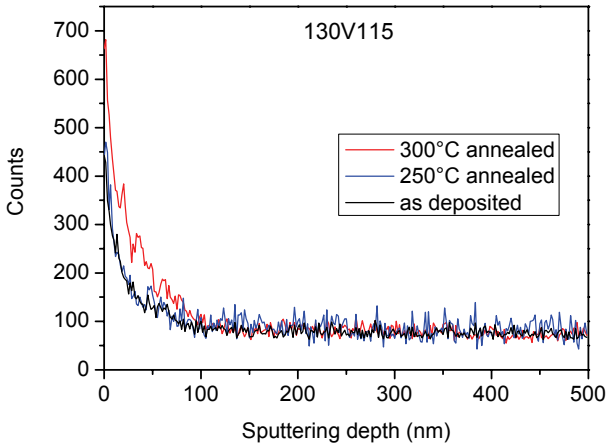

Figure 6.20 *Auger depth-profiling of oxygen element in the coating 130V115 after annealing at different temperatures in comparison with that of the as-deposited coating.*

above 300°C. In addition, the coatings annealed at higher temperatures exhibit a higher CoF at the onset of a tribo-test and need longer time to reach the low steady-state CoF. For instance, the peak CoF at the beginning of sliding for the coatings annealed at 350 °C is twice as high compared with the values measured for coatings annealed below 250 °C. In other words, annealing at higher temperatures deteriorates the self-lubrication effect. In particular, the coatings with higher carbon content such as 130V120 are influenced more dramatically by annealing (Fig. 6.19), which can be attributed to the oxidation of the DLC matrix material.

Auger depth profiles of the oxygen concentration in the as-deposited and annealed 130V115 coating is shown in Fig. 6.20 and reveals that oxidation of TiC/DLC coatings during one hour annealing in air is negligibly small up to the annealing temperature of 250 °C. A substantial increase in oxygen content has been detected after annealing at 300 °C. However, the diffusion depth of oxygen is limited to about 100 nm in the annealed coating. Annealing for a longer time or at higher temperatures will increase further the oxygen content as well as the diffusion depth in the coatings, which may result in heavier degradation of the annealed coatings. This oxidation behavior of a thin surface layer explains the higher initial CoF and the longer transition period needed to reach the steady-state CoF for the coatings annealed at higher temperatures. Indeed, a CoF value as high as 0.28 was observed for coating 0V110 that contains 16 at. % oxygen.

TRIBOLOGICAL BEHAVIOR AT ELEVATED TEMPERATURE

Ball-on-disk tribo-tests were performed starting at room temperature and gradually increasing the temperature during the test. The ultra-low friction regime of TiC/DLC coatings may maintain up to 200°C, as shown in Fig. 6.21, where the CoF (~0.01) is lower than the steady-state CoF of the coating tested at room temperature. The friction coefficient

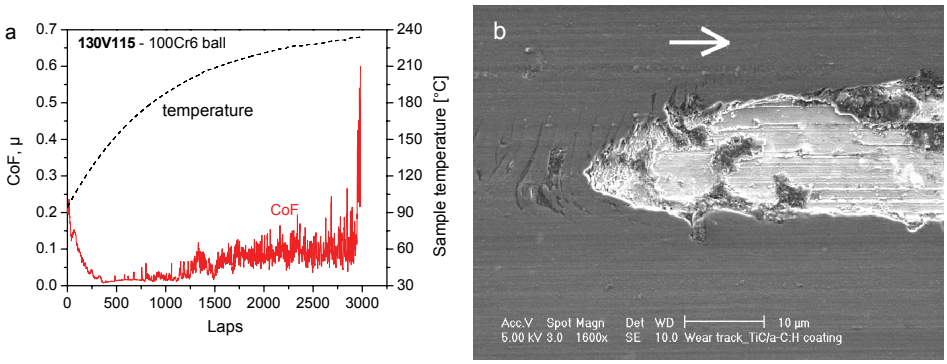

Figure 6.21 *Elevated temperature tribo-testing results of the coatings: (a) 130V115 tested in air of 50% relative humidity, 5 N normal load, 10 cm/s sliding velocity). SEM micrograph of the middle part of the wear track on the coating 130V115 showing a damaged spot where the coating delaminated during the elevated-temperature tribo-test. An arrow indicates the moving direction of the ball counterpart.*

gradually increases to a value of 0.1 as the temperature rises above 200 °C. Thereafter, the coating suddenly fails at about 230°C with a sliding life shorter than 3000 laps (revolutions), indicated by a peak in the friction trace up to a value of about 0.6. The latter is a typical CoF value for dry sliding between metal-to-metal contacts. This indicates that coating delamination is the failure mechanism, as confirmed by SEM observations in Fig. 6.21b.

The two different levels of CoF before abrupt failure of the coating deserve special comments. At the early stage of a test the CoF drops to a very low value of about 0.01 as the sample temperature rises rapidly towards 100 ˚C. This phenomenon is attributed to the gradual desorption of water molecules from the sliding surfaces with increasing temperature, whose effect is equivalent to that of decreasing the humidity level of the atmosphere. When the sample temperature is above 200 °C, the coating surface oxidizes locally at the hot spots on sliding contact where the peak temperature may be well above 350 °C. This leads to an increase in oxygen content in the top atomic layers of the coatings and consequently a significant increase in CoF, close to the CoF value of the annealed coatings. In addition, the 100Cr6 ball counterpart starts to soften at such high temperatures, which may destroy the transfer films and lead to adhesive wear due to the higher friction coefficient. Ultimately it results in delamination of the coating as observed in Fig. 6.21b.

6.6.2 HYDROGEN-FREE DLC COATINGS

Tribo-tests were performed at 0.3 m/s sliding speed and 5 N normal load, in an atmosphere of relative humidity (RH) in the 50-60 % range. For tests at ambient temperature, different 6 mm Ø ball counterparts (100Cr6 steel (AISI 52100), Si_3N_4, Al_2O_3) were used, while high-temperature tests were performed against an Al_2O_3 counterpart.

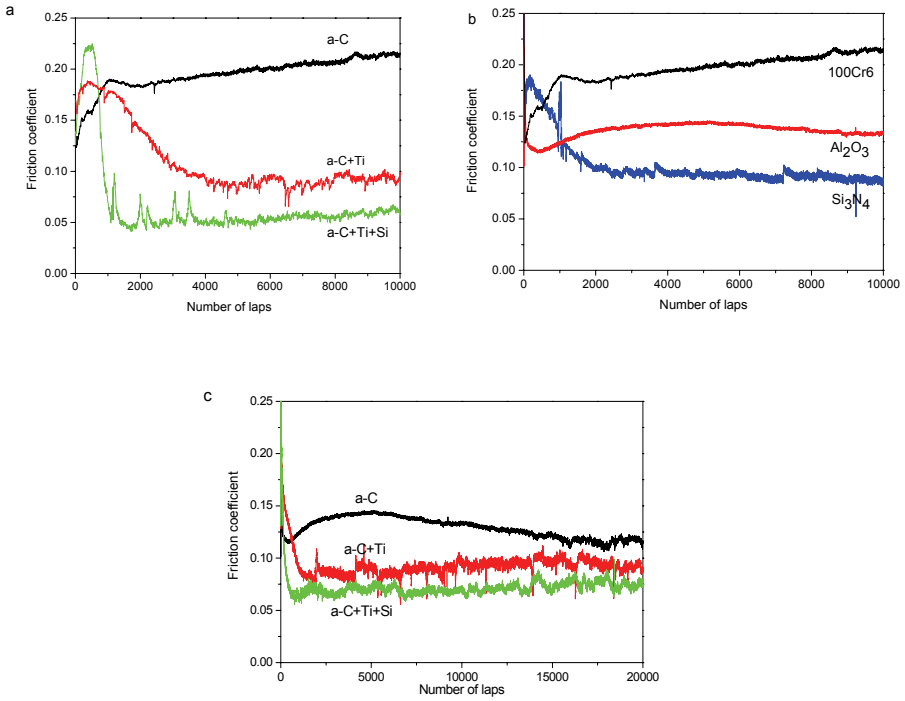

Figure 6.22 *(a) Graphs of friction coefficient versus number of laps tested at sliding velocity of 30 cm/s: (a) all coatings sliding against a 100Cr6 ball, (b) a-C coating sliding against different counterparts. (c) all coatings sliding against an Al_2O_3 counterpart.*

The evolution of the friction coefficient during tribological tests against the 100Cr6 steel ball is shown in Fig. 6.22a. The addition of Ti and Si to the DLC material decreases the friction coefficient. For comparison, it was observed by Strondl et al.[17] that the addition of W to DLC coatings resulted in an increase of the friction coefficient. The values of the wear rate measured from the wear track profiles are 3, 5 and 7 $\times 10^{-8}$ [mm^3/N m lap] for the a-C, the a-C+Ti and the a-C+Ti+Si coatings, respectively. A slight increase of wear rate is observed as alloying elements are added to the material, as shown in table 6.3.

Table 6.3: *Chemical composition, hardness (H), reduced Young's modulus (E*), wear rate (W) and coefficient of friction (CoF) of the coatings.*

Coating	Ti [at. %]	Si [at. %]	H [GPa]	E* [GPa]	W [mm^3/N m lap]
a-C	-	-	26.2	220.8	3×10^{-8}
a-C+Ti	11	-	18.4	186.8	5×10^{-8}
a-C+Ti+Si	14	5	18.7	194.3	7×10^{-8}

The tribological behavior of the pure DLC coatings was investigated against different counterpart materials, as depicted in Fig. 6.22b. The counterpart material influences the friction coefficient considerably; nevertheless, when the different coatings are tested against the same counterpart material (Al_2O_3) in Fig. 6.22c, the evolution of friction coefficient with the composition is consistent with the observations of the 100Cr6 counterpart.

ELEVATED TEMPERATURE TRIBOTESTS

To avoid a possible influence of the temperature on the hardness of the 100Cr6 ball the high temperature tribological tests were performed for all the coatings against an Al_2O_3 ball. The tests started at room temperature, and during the tests the coatings temperature was gradually increased from ambient to 300 °C. The experiments were immediately stopped when a sudden increase of friction coefficient was observed, and the relative temperature was taken as the maximum working temperature for each coating material under the test conditions, as indicated in Fig. 6.23. Interestingly, all the coatings exhibited a lower friction coefficient at high temperature than at ambient temperature, and the maximum working temperatures of the a-C, a-C+Ti and a-C+Ti+Si coatings were 285 °C, 210 °C and 160 °C, respectively.

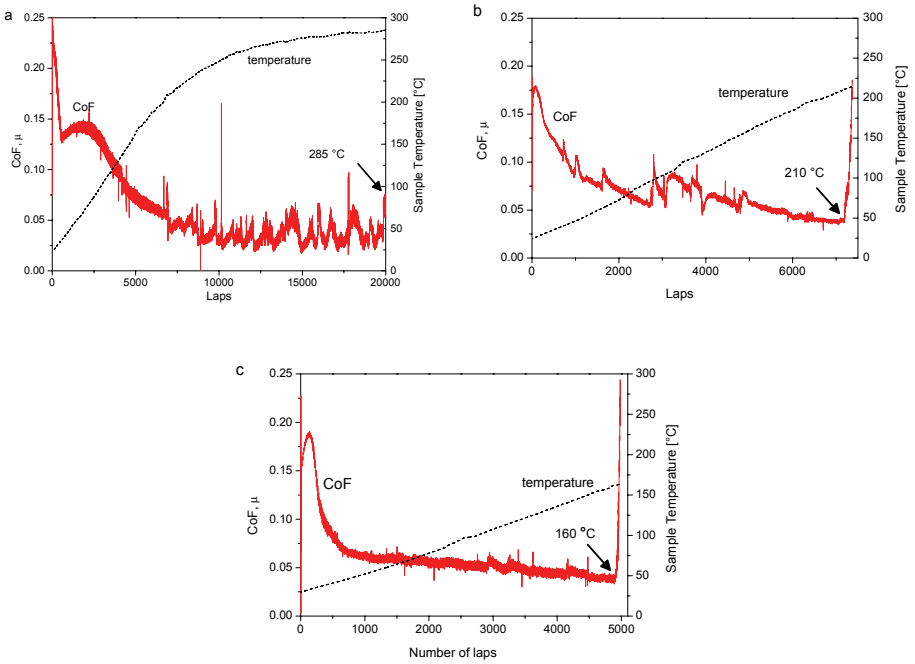

Figure 6.23 *Evolution of coefficient of friction (COF) and temperature (T) as a function of the number of laps for an Al_2O_3 ball sliding against (a) the a-C coating (b) the a-C+Ti coating (c) the a-C+Ti+Si coating. Tests performed at 30 cm/s sliding velocity and 5 N applied load.*

It was shown in section 6.6.1 and known from literature that DLC-based coatings are stable under annealing in air up to temperatures of at least 250 °C.[18, 19] Nevertheless, it has been shown that a degradation mechanism is present during the elevated temperature tribo-tests that limit their use to lower temperatures. After each test was stopped, the wear track was checked with an optical microscope and an SEM. No delamination was observed, but instead wear debris was present on the surface of all coatings. The wear debris was compacted and formed an adherent transfer layer on the wear track (reverse transfer layer). The coverage of the reverse transfer layer on the surface of the coatings increased strongly as Ti and, subsequently, Si, were added as alloying elements. In Fig. 6.24a the reverse transfer layer is observed in the central part of the wear track for the a-C+Ti+Si coating. The nature of the reverse transfer layer was further investigated in an SEM. Its morphology is shown in Fig. 6.24b, and the EDX analysis of its composition is reported in Fig. 6.24c. The EDX analysis indicates that it consists of oxidized coating material, including traces of Al from the ruby counterpart. The presence of compacted wear debris over the surface of the coatings is likely to disrupt the self-lubricating effects. If the tests were continued after the formation of the transfer layer, delamination occurred because of the higher sliding friction coefficient, leading quickly to the total failure of the coatings. The formation of the reverse transfer layer is enhanced by the presence of alloying elements in the coatings, and pure a-C coatings provide a low friction coefficient up to a temperature of 285 °C.

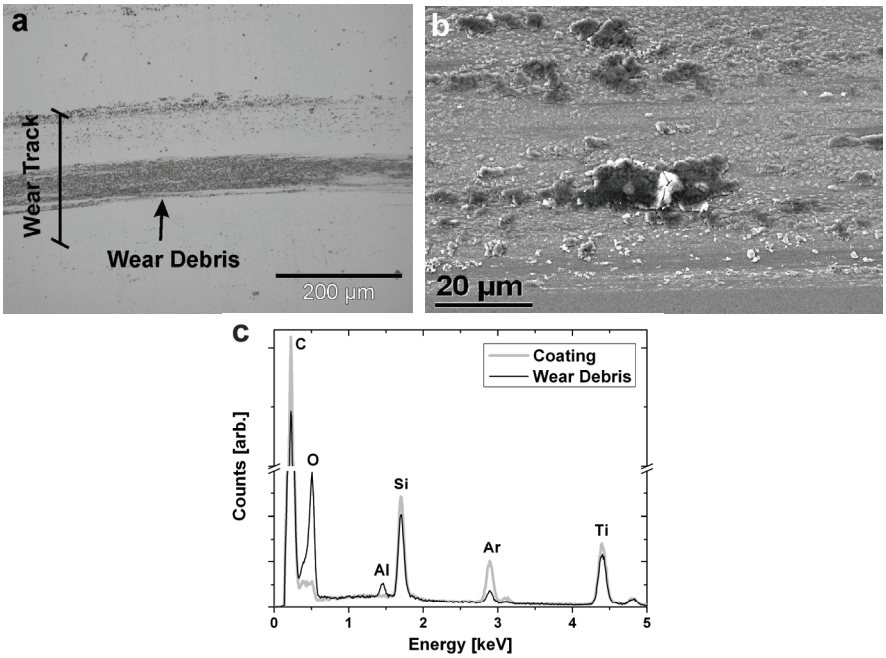

Figure 6.24 *(a) Optical microscope images of the wear tracks of the Ti/Si alloyed a-C coating. (b) SEM magnification of a detail from the wear debris area. (c) EDX spectra of the compositional differences between the coating and the wear debris.*

6.7 CONCLUSIONS

TiC/DLC nanocomposite coatings manifest strong self-lubricating effects during sliding wear tests, combining ultra-low friction with superior wear resistance. The lowest wear rate values were always observed for the coatings with the lowest V_F of TiC particles. The lowest values of the friction coefficient were found at intermediate values of TiC V_F. As a consequence it is possible to trade-off wear resistance for lower friction coefficient, depending on whether the final application demands high wear resistance or low friction as primary requirements.

The results of tribological investigations point to a breakdown of the Coulomb friction law for self-lubricating TiC/hydrogenated DLC nanocomposite coatings, where lower friction coefficients are observed at higher sliding velocities. This effect is due to the adsorption of water vapor over the coating surface, which increases the friction coefficient. This effect is enhanced at lower sliding velocity. Indeed, the CoF of the self-lubricating coatings decreases with decreasing relative humidity of the testing atmosphere.

TiC/hydrogenated DLC coatings are stable after annealing in air up to a temperature of at least 250 ˚C. No variation of their mechanical properties or appreciable oxidation was observed. Its wear resistance also remained unchanged up to this temperature. Nevertheless, tribological tests at high temperature resulted in failure of the self-lubrication mechanism and subsequent coating failure at temperatures around 200 ˚C.

The introduction of alloying elements in H-free DLC coatings reduces their hardness and their wear resistance, but decreases considerably the sliding friction coefficient at ambient temperature. Chemical alloying is therefore an efficient approach to vary the properties of DLC coatings for different applications. Nevertheless, care should be taken when selecting DLC coatings for applications at elevated temperatures. Indeed, in the higher temperature range all coatings provide lower friction coefficients than typically observed at ambient temperature. Pure DLC coatings are able to provide a sliding friction coefficient below 0.1 during sliding at high temperature up to 285 °C, while the presence of Ti and Si alloying elements may decrease the maximum operating temperature of the coatings to 160 °C.

References

1. I.L. Singer, Langmuir **12**, 4486 (1996).
2. J. Robertson, Mater. Sci. Eng. R **37**, 129 (2002).
3. H. Zaïdi, D. Paulmier and J. Lepage, Appl. Surf. Sci. **44**, 221(1990).
4. J.A. Heimberg, K.J. Wahl, I.L. Singer and A. Erdemir, Appl. Phys. Lett. **78**, 2449 (2001).
5. H. Blok, Proc. Inst. Mech. Eng. London, Vol. **2**, 222 (1937).
6. F.P. Bowden and P.H. Thomas. Proc. Roy. Soc. A **223**, 29 (1954).
7. X.F. Tian and F.E. Kennedy. J. Tribology **116**, 167 (1994).
8. E. Rabinowicz. Friction and Wear of Materials, John Wiley and Sons, New York, (1965), p.86-90; 2nd Ed. (1995), p.99-100.
9. P. Daguier, G. Baudry, J. Bellus, G. Auclair, J. Rofès-Vernis, G. Dudragne, D. Girodin and G. Jacob. In: Bearing Steel Technology, Proc. 6th Int. Symp. Bearing Steels, ASTM STP 1419, Ed. J.M. Beswick, American Society for Testing Materials, West Conshohocken, PA (2001).
10. C. J. Morath, H. J. Maris, J.J. Cuomo, D.L. Pappas, A. Grill, V.V. Patel, J.P. Doyle, K.L. Saenger, J. Appl. Phys. **76**, 2636 (1994).

11. A.J. Bullen, K.O'Hara, D. G. Cahill, O. Monteiro, A. Von Keudell, J. Appl. Physics **88**, 6317 (2005).
12. R. Landauer, J. Appl. Phys. **23**, 779 (1952).
13. F. W. Smith, J. Appl. Phys. **55**, 764 (1984).
14. S.Y. Elovich, G. M. Zhabrova, Zh. Fiz. Khim **13**, 1761 (1939).
15. K. Tamaru, Trans. Faraday Soc. **59**, 979 (1963).
16. P.W. Atkins, Physical Chemistry, Oxford University Press (1998).
17. C. Strondl, G.J. van der Kolk, T. Hurkmans, W. Fleischer, T. Trinh, N.M. Carvalho, J.Th.M. De Hosson, Surf. Coat. Technol. **142-144**, 707 (2001).
18. D.R. Tallant, J.E. Parmeter, M.P. Siegal, R.L. Simpson, Diam. Relat. Mater. **4**, 191 (1995).
19. B.K. Tay, D. Sheeja, S.P. Lau, X. Shi, B.C. Seet, Y.C. Yeo, Surf. Coat. Technol. **130**, 248 (2000).